MASS EXTINCTION

Thresholds of catastrophe in the Earth system

Daniel H. Rothman

The history of the Earth system is a story of change. Some changes are gradual and benign, but others, especially those associated with catastrophic mass extinction, are relatively abrupt and destructive. What sets one group apart from the other? Here, I hypothesize that perturbations of Earth's carbon cycle lead to mass extinction if they exceed either a critical rate at long time scales or a critical size at short time scales. By analyzing 31 carbon isotopic events during the past 542 million years, I identify the critical rate with a limit imposed by mass conservation. Identification of the crossover time scale separating fast from slow events then yields the critical size. The modern critical size for the marine carbon cycle is roughly similar to the mass of carbon that human activities will likely have added to the oceans by the year 2100.

INTRODUCTION

Five times in the Phanerozoic [the past 542 million years (My)], more than three-fourths of marine animal species have vanished in mass extinctions (*1*). Each of these events is associated with a significant change in Earth's carbon cycle (*2*, *3*). However, there are a great many disturbances of the carbon cycle (*3*, *4*) whose imprint in the geologic record is almost exclusively environmental. These other events are relatively benign, with extinction rates barely, if at all rising, above background levels (*5*–*7*).

Two well-studied examples illustrate these distinctions. The end-Permian extinction [~252 million years ago (Ma)], the most severe mass extinction in the Phanerozoic (*8*), plays out over a period of 10^4 to 10^5 years; the extinction interval immediately follows a perturbation of the carbon cycle of similar duration (*9*). The Paleocene-Eocene Thermal Maximum (~55.5 Ma) is a carbon cycle event of roughly similar time scale, with unambiguous signs of global warming and ocean acidification (*10*, *11*). It is associated with a significant extinction of benthic foraminifera (*12*, *13*), but there is no evidence of other major extinctions (*11*, *13*, *14*). What makes these two events so different? The unambiguous co-occurrence of the end-Permian extinction with massive volcanism (*15*) provides one indication, as does the greater magnitude of the end-Permian carbon isotopic excursion compared to that of the Paleocene-Eocene Thermal Maximum (*10*, *16*). However, no general distinction, applicable throughout the Phanerozoic, exists (*5*–*7*).

The idea that mass extinction results from catastrophic environmental change was largely developed more than two centuries ago by Cuvier (*17*). But what defines such an environmental catastrophe? Newell (*18*) implicitly provides a practical definition: "Extinction… is not simply a result of environmental change but is also a consequence of failure of the evolutionary process to keep pace with changing conditions in the physical and biological environment" (*18*). In other words, catastrophe results when the rate of environmental change exceeds a threshold.

To consider such ideas within the context of the carbon cycle, suppose that the mass m of inorganic carbon in the oceans is increased from its steady-state value, m^*, by an amount Δm over a duration τ_{env} of time. In terms of the relative change $M = \Delta m/m^*$, Newell's statement hypothesizes that mass extinction results when M/τ_{env} exceeds a critical rate r_c. However, one recognizes immediately that this condition cannot apply for impulsive change as $\tau_{env} \to 0$. In this case, M must instead exceed a finite critical size M_c. Putting it all together, catastrophe follows when

$$M > \begin{cases} M_c, & \tau_{env} \ll \tau_x \quad (1) \\ r_c \tau_{env}, & \tau_{env} \gg \tau_x \quad (2) \end{cases}$$

where τ_x is the crossover time scale separating fast from slow change. Because the asymptotic regions 1 and 2 intersect at $\tau_{env} = \tau_x$, the three unknowns M_c, r_c, and τ_x can be assumed to satisfy

$$M_c = r_c \tau_x \quad (3)$$

In principle, Eq. 3 shows how the record of slow environmental change at geologic time scales informs our understanding of rapid change at human time scales, even though mechanisms at the different time scales may differ. Here, I provide an analysis of the geological record that makes contact with this picture.

RESULTS

I begin by constructing an empirical database of significant global perturbations of Earth's carbon cycle during the Phanerozoic. Each perturbation is considered to be an isolated event, or excursion, in the evolution of the isotopic composition δ_1 of inorganic (carbonate) carbon. Except for the most recent event (beginning at the Last Glacial Maximum), the analysis focuses exclusively on isotopic changes that decrease δ_1. Each isotopic event is parameterized as shown in Fig. 1A.

The database contains each event's geologic age, the time τ_{env} over which δ_1 decreases, and the isotopic compositions $\delta_1(0)$ and $\delta_1(\tau_{env})$ that bracket the change from time $t = 0$ to $t = \tau_{env}$. Whenever possible, estimates of τ_{env} are obtained from isotope geochronology or astrochronology. The compilation contains a total of 31 events distributed throughout the Phanerozoic (Fig. 1B), including each of the so-called Big Five mass extinctions. The resulting data are contained in Table 1. Further information is available in Materials and Methods.

Figure 2A displays the isotopic response $\Delta_r = \delta_1(\tau_{env}) - \delta_1(0)$ of each event as a function of its time scale τ_{env}. Two features of the data immediately stand out. First, there is a relative absence of large excursions at short time scales, suggesting that there may be a characteristic limitation to the rate at which the marine inorganic carbon reservoir can change its isotopic composition. Second, four of the Big Five mass

Lorenz Center, Department of Earth, Atmospheric, and Planetary Sciences, Massachusetts Institute of Technology, Cambridge, MA 02139, USA. Email: dhr@mit.edu

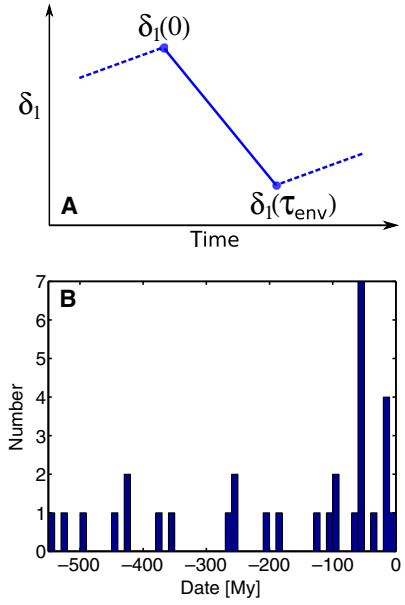

Fig. 1. Parameterization and temporal distribution of carbon isotopic events in the database. (**A**) Schematic diagram illustrating how the parameters $\delta_1(0)$ and $\delta_1(\tau_{env})$ are derived from an isotopic time series $\delta_1(t)$. The time scale τ_{env} represents the duration of time during which the isotopic composition δ_1 decreases. (**B**) Histogram depicting the distribution of events in time.

extinctions appear to exhibit anomalously fast rates of change. The fifth mass extinction, in the late Devonian at the Frasnian-Famennian boundary, is clearly different, lying in the slow region in the lower right-hand corner (labeled "FF"). McGhee (*19*) and Bambach *et al.* (*20*) have suggested that the Frasnian-Famennian event is not an extinction event but instead represents a decrease in the rate at which new species originate. Its relatively small and slow isotopic perturbation provides indirect support for this idea.

To understand these observations more deeply, I transform the geochemical changes to physical fluxes (Materials and Methods). The transformation assumes that the global carbon cycle is composed of two reservoirs: inorganic and organic carbon. Carbon is exchanged between the two reservoirs by photosynthesis and respiration. Inorganic carbon of isotopic composition δ_i enters the cycle with flux j_i. Both inorganic and organic carbon exit the cycle when buried as rock.

The downturn of δ_1 is assumed to be driven by a time-dependent flux $j_i'(t)$ of inorganic carbon with isotopic composition δ_i', which is set equal to the average Phanerozoic isotopic composition of organic carbon [− 27.8‰ (*21*)]. In other words, j_i' represents an imbalance in the loop between photosynthesis and respiration on time scales up to τ_{env}. Its origin is unspecified, but its growth is assumed to be linear. Taking each event to begin at $t = 0$ and defining the normalized flux $J(t) = j_i'/j_i^*$, where j_i^* is the unperturbed input flux, one then has

$$J(t) = \phi t/\tau_{env}, \qquad 0 \le t \le \tau_{env} \tag{4}$$

where ϕ is an unknown, event-specific, dimensionless constant that specifies the maximum normalized flux $J(\tau_{env})$. An alternative model could be a constant perturbation $J = \phi$. But such a choice would result in equilibration to a new steady state in the many instances in which τ_{env} is greater than the turnover time $\tau_0 = m^*/j_i^* = 140$ ky (thousand years) (Materials and Methods). The analysis here instead assumes that perturbations grow until $t = \tau_{env}$. The linear model (Eq. 4) can therefore be viewed as a first-order approximation of a flux function that satisfies this condition. The normalized mass M in Eqs. 1 and 2 derives from its integral:

$$M(\phi,\ \tau_{env}) = \frac{1}{\tau_0}\int_0^{\tau_{env}} J(t)\mathrm{d}t = \frac{\phi\tau_{env}}{2\tau_0} \tag{5}$$

To determine the flux $J(t)$ consistent with each isotopic event, I calculate the value of ϕ that solves differential equations for the evolution of $\delta_1(t)$, $M(t)$, and $J(t)$ given the initial values $\delta_1(0) = \delta_1^*$, $J(0) = 0$, and $M(0) = 0$ and the final value $\delta_1(\tau_{env}) = \delta_1^* + \Delta_r$. The values of δ_1^*, Δ_r, and τ_{env} are obtained for each event from the database. The solution of this boundary value problem for ϕ provides the evolution of $\delta_1(t)$ that matches its observed initial and final states while remaining consistent with differential equations describing changes in the isotopic composition of marine inorganic carbon in response to the flux $J(t)$. It also provides, via Eqs. 4 and 5, the rate at which J grows and thus the mass M.

Figure 2B shows M as a function of τ_{env}, rescaled according to Eq. 5, for each event. The gross features seen in the raw data of Fig. 2A remain, but now, the appearance of a limiting rate, suggested once again by the relatively barren upper-left half of the plot, is sharper. Moreover, the limiting rate now has a physical interpretation. From Eq. 4, one sees that the normalized flux perturbation reaches its maximum value, $J = \phi$, when $t = \tau_{env}$. The limiting rate therefore represents a critical dimensionless flux ϕ_c beyond which the carbon cycle rarely ventures. When it does, mass extinction often follows.

I hypothesize that ϕ_c derives from organic carbon that would normally be buried as rock but is instead converted to CO_2 and remobilized into the marine carbon cycle. The rate of this remobilization can be no greater than the rate at which organic carbon is immobilized (that is, buried) in an unperturbed steady state. During the Phanerozoic, this limiting rate equals 23 ± 7% of the steady input (or output) flux j_i^* (Materials and Methods). Therefore, $\phi_c = 0.23$ is the maximum possible normalized flux perturbation in a mass-conserving carbon cycle with no anomalous sources or sinks. The straight line in Fig. 2B, which shows $M(\phi_c, \tau_{env})$ as defined by Eq. 5, represents this hypothesis quantitatively.

This line separates two kinds of carbon cycles. Below the line, perturbations can be explained by a partial cessation of organic carbon burial. Above the line, they cannot. On the line, the small leak represented by burial is temporarily closed when the perturbation reaches its maximum strength at $t = \tau_{env}$. Roughly half of the events in the database fall within the error bars of this boundary. Four of the Big Five mass extinctions lie above the upper error bar, whereas nearly all other events fall below it. These observations suggest that noncatastrophic perturbations represent flux changes along a fixed set of pathways, whereas catastrophic perturbations result from the introduction of new pathways acting as anomalous sources or sinks. I refer to the borderline perturbations as critical events. The preponderance of critical events supports the idea that large yet benign flux perturbations tend to grow until their source—the small fraction of organic matter that would normally be destined for burial—is fully depleted via respiration.

The critical events are likely driven to their limit by the intrinsic dynamics of the carbon cycle over a time scale set by the characteristic relaxation time associated with a negative feedback. However, the variation of τ_{env} over 10^4 to 10^6 years would seem to rule out a unique damping mechanism. This disqualification would necessarily hold if the carbon cycle did not change over geologic time. But evidently it

Table 1. Event names, event abbreviations, and data used to construct Figs. 2 and 3. Values of δ_1 and Δ_r are given in per mil (‰) and derive from the formula $\delta_1 = 1000 \times (R - R_{std})/R_{std}$, where abundance ratios $R = {}^{13}C/{}^{12}C$ are obtained from samples of inorganic (carbonate) carbon and R_{std} is a standard ratio. The variables Δ_r, τ_{env}, ϕ, and M are defined in the text. In Fig. 2, the six Eocene and four Miocene events are denoted by Eo and Mio, respectively.

Event name	Abbreviation	Date[Ma]	$\delta_1(0)$	$\delta_1(\tau_{env})$	Δ_r	τ_{env}[My]	ϕ	M
Ediacaran-Cambrian	Edi	541.00	2.50	−4.00	−6.50	2.000	0.32	2.302
Nemakit-Daldynian-Tommotian	NDT	524.36	5.00	−3.00	−8.00	0.982	0.41	1.450
Cambrian Spice	Spice	497.00	4.30	1.30	−3.00	1.000	0.12	0.443
End-Ordovician	Ord	445.80	4.90	−0.70	−5.60	0.230	0.42	0.344
Silurian Mulde	Mul	428.20	4.00	1.00	−3.00	0.260	0.19	0.181
Silurian Lau	Lau	423.50	7.00	1.00	−6.00	0.500	0.30	0.538
Frasnian-Famennian	FF	372.20	3.50	2.00	−1.50	1.540	0.06	0.311
Tournaisian	Tou	351.55	5.60	2.10	−3.50	1.510	0.13	0.727
Mid-Capitanian	Cap	262.45	4.00	−1.00	−5.00	0.500	0.27	0.480
End-Permian	PT	251.94	4.00	−1.50	−5.50	0.060	1.13	0.243
Early Triassic	Tr	251.22	2.00	−1.50	−3.50	0.250	0.26	0.228
Triassic-Jurassic	TJ	201.64	0.00	−2.00	−2.00	0.050	0.49	0.087
Toarcian	Toar	182.60	2.10	−0.90	−3.00	0.150	0.29	0.157
Aptian	Apt	120.21	2.95	1.80	−1.15	0.047	0.26	0.043
Albian-Cenomanian	Al/Cn	100.50	2.50	1.80	−0.70	0.110	0.08	0.030
Mid-Cenomanian	mCn	95.90	3.10	2.25	−0.85	0.138	0.08	0.038
Cenomanian-Turonian	CT	94.20	5.30	3.70	−1.60	0.553	0.07	0.135
Cretaceous-Paleogene	KT	65.50	3.13	1.98	−1.15	0.026	0.44	0.041
Early late Paleocene	ELPE	58.90	3.48	3.07	−0.42	0.039	0.11	0.015
Paleocene-Eocene Thermal Maximum	PETM	55.50	1.90	−0.80	−2.70	0.083	0.41	0.121
Eocene Thermal Maximum 2	ETM2	53.70	1.40	0.27	−1.12	0.045	0.28	0.045
Eocene Hyperthermal H2	H2	53.60	1.40	0.80	−0.60	0.033	0.19	0.023
Eocene Hyperthermal I2	I2	53.20	1.56	0.95	−0.61	0.040	0.16	0.023
Eocene Hyperthermal I1	I1	53.10	1.56	0.84	−0.72	0.040	0.19	0.028
Eocene Thermal Maximum 3	ETM3	52.50	0.20	−0.60	−0.80	0.037	0.24	0.032
Eocene-Oligocene boundary	Oi1	33.50	1.60	1.00	−0.60	0.430	0.03	0.047
Miocene Climatic Optimum 1	MCO1	16.90	1.94	1.44	−0.50	0.028	0.18	0.018
Miocene Climatic Optimum 2	MCO2	16.40	1.80	1.04	−0.76	0.022	0.35	0.028
Miocene Climatic Optimum 3	MCO3	16.00	2.33	1.67	−0.66	0.032	0.21	0.024
Miocene Climatic Optimum 4	MCO4	15.60	2.17	1.57	−0.60	0.029	0.21	0.022
Last Glacial Maximum–to–Holocene	LGMH	0.02	0.11	0.45	0.34	0.018	−0.20	−0.013

did: Fig. 3A shows that the upper envelope of event size M decreases with time. To understand this evolution, note that Eq. 5 predicts that changes in the size of critical events, for which $\phi = \phi_c$, derive directly from changes in τ_{env}. Figure 3B shows that this time scale—which should be roughly equivalent to the damping time—decreases toward the present.

The time scale of critical events appears to have declined since the early Triassic (~250 Ma) by about one order of magnitude, to about 20 to 30 ky since the Miocene (~16 Ma). The smaller time scale is similar to the ~10-ky time scale of the modern oceans' homeostatic response to a change in pH (*22*–*25*). The time scale's decrease since the Triassic is consistent with the evolutionary expansion of the modern biological

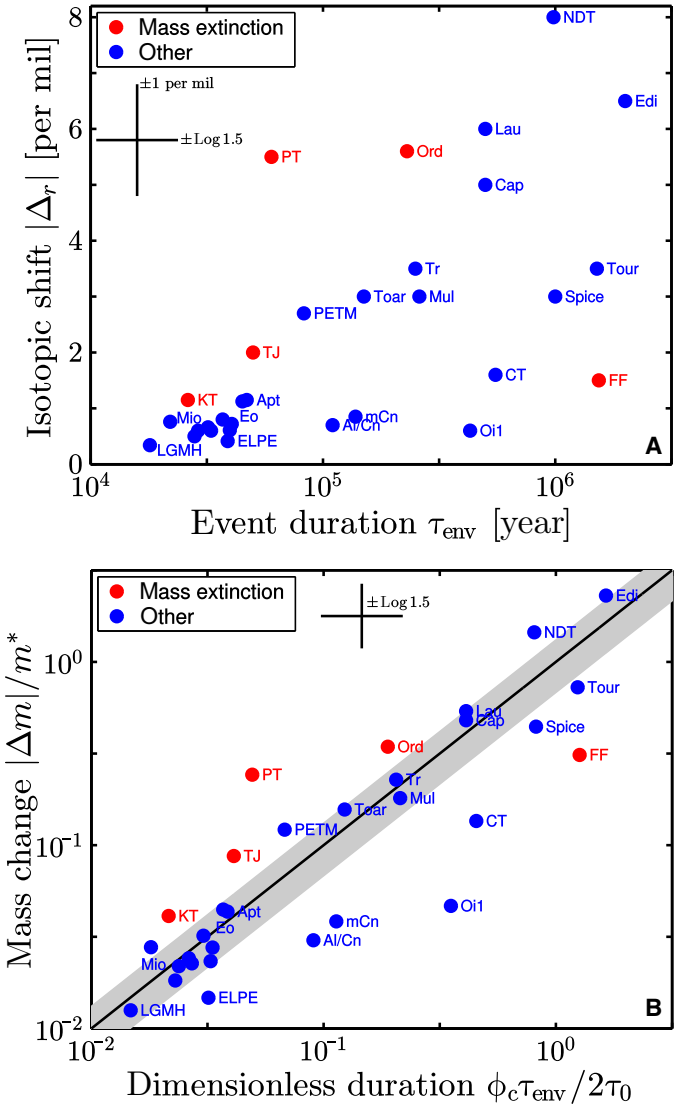

Fig. 2. Depictions of the size and time scale of carbon isotopic events. (**A**) Magnitude of the isotopic shift $\Delta_r = \delta_1(\tau_{env}) - \delta_1(0)$ as a function of its duration of time, τ_{env}. (**B**) Dimensionless mass perturbation $M = |\Delta m|/m^*$ as a function of the dimensionless time scale $\phi_c\tau_{env}/2\tau_0$ for each of the events depicted in (A). The straight (identity) line denotes the equality predicted by Eq. 5 when $\phi = \phi_c = 0.23 \pm 0.07$. Event abbreviations are defined in Table 1. Error bars (Materials and Methods) are guides for interpretation.

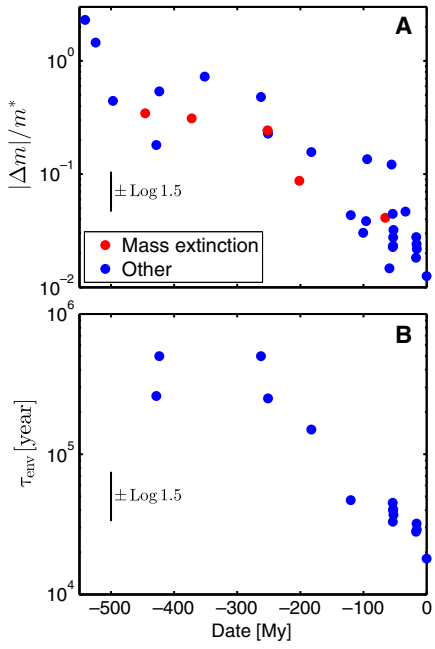

Fig. 3. Evolution of size and time scale. (**A**) Dimensionless mass perturbation $M = |\Delta m|/m^*$ as a function of the geologic age of the event. The relative absence of smaller events in the deeper past likely derives from poor data and a lack of interest. The absence of large events in the more recent past, however, cannot be explained by this bias. (**B**) Time scale τ_{env} of critical events (events falling within the error bars of the straight line in Fig. 2B) as a function of geologic age. Error bars (Materials and Methods) are guides for interpretation.

pump beginning approximately 220 Ma (*26*, *27*), corresponding to the earliest observations of coccolithophores and associated calcareous phytoplankton in the fossil record (*28*, *29*). As the biological pump strengthened, the export of precipitated calcium carbonate from surface waters to deep ocean sediments increased, leading to growth of the deep-sea sedimentary carbonate reservoir (*26*, *27*, *30*). When pH decreases in modern oceans, dissolution of sedimentary carbonate minerals is one of the principal processes via which these disturbances are damped (*31*, *32*). Because this mechanism strengthened over the last 220 My, critical perturbations of the marine carbon cycle would have become shorter in time and smaller in magnitude, but not necessarily less dangerous, because their maximum flux would have remained ϕ_c. These observations are each consistent with the suggestion that the carbon cycle became less variable after the introduction of the deep-sea carbonate sink (*26*, *27*, *30*, *33*). They also identify the crossover time scale τ_x with the homeostat time scale, implying $\tau_x \sim 10$ ky (*22*–*25*) in modern oceans.

With these results in hand, the modern critical size M_c of an asymptotically fast perturbation of the marine carbon cycle now follows. First, insertion of $M(\phi_c, \tau_{env})$ from Eq. 5 into Eq. 2 provides the critical rate $r_c = \phi_c/2\tau_0$. Equation 3 then predicts

$$M_c = \frac{\phi_c \tau_x}{2\tau_0} \quad (6)$$

$$= 0.0082 \pm 0.0041 \quad (7)$$

where, as a guide, a total uncertainty of ±50% is assumed. The modern oceans contain about 38,000 Pg C; the critical dimensional mass is therefore about 310 ± 155 Pg C.

From 1850 to the present, human activities have resulted in the addition of about 155 ± 25 Pg C to the oceans (*34*). Projections for further carbon uptake depend strongly on the trajectory of fossil fuel emissions and land use, among other factors (*34*, *35*). Figure 4 compares the critical mass to the present accumulation and four projections to 2100 obtained from coupled climate–carbon cycle models (*34*). The strictest emission scenario results in oceanic carbon uptake whose mean falls just below the critical mass; at the other extreme, the mean model uptake is about 74% greater than critical. Although the uncertainty of each prediction in Fig. 4 is considerable, all scenarios for cumulative uptake at the century's end either exceed or are commensurate with the threshold for catastrophic change.

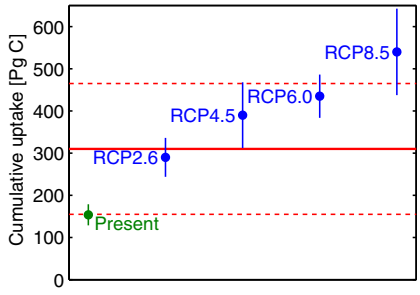

Fig. 4. Cumulative modern ocean uptake of carbon since 1850, up to the present (green) and projected to 2100 (blue), compared to the predicted critical mass of 310 Pg C (solid red line) and an assumed uncertainty of ±50% (dashed red lines). Projections (*34*) are given for four representative concentration pathway scenarios RCP*x*, where *x* represents the radiative forcing, in units of W/m^2, deriving from accumulated emissions in the year 2100 (*35*). At the extreme ends of the projections, RCP2.6 represents the range of lowest-emission scenarios in the scientific literature, and RCP8.5 represents the high range of nonclimate policy scenarios. Of the two intermediate pathways, RCP4.5 corresponds to an emission pathway resulting from many climate policies found in the literature, whereas RCP6.0 is representative of most scenarios without limitations on emissions (*35*). The present cumulative uptake is obtained by adding 6 years of an annual uptake rate of 2.3 Pg C year^{-1} (*34*) to the 2011 total of Ciais *et al.* (*34*).

DISCUSSION

The value of the empirical results in Figs. 2 and 3 lies not in any individual data points but rather in their collective trends. The following picture emerges. Carbon isotopic events rarely exceed a maximum isotopic shift that grows roughly like the logarithm of their time scale. This upper bound appears related to the minimum rate—zero—at which organic carbon can be immobilized as rock. Events outside this limit result from a fundamental disturbance of the carbon cycle, possibly related to unstable dynamics, mass extinction, or both.

These conclusions follow from analyzing all isotopic events the same way. Exceptions are, however, expected. For example, four events (Ediacaran-Cambrian, Nemakit-Daldynian-Tommotian, Paleocene-Eocene Thermal Maximum, and Miocene Climatic Optimum 2) unaccompanied by mass extinction exceed the upper error bar of the critical rate. If, say, these events were driven by dissociation of methane hydrates [for example, (*36*)] rather than respired organic carbon, the isotopic composition of the perturbative flux would be much lighter (about −60‰). The estimated size of these events would then drop by more than 50%, and they would each lie below the critical line. This observation may help explain the Paleocene-Eocene Thermal Maximum's modest biotic impact. The Frasnian-Famennian extinction provides another exception. Supposing that it is indeed a mass extinction, its presence well below the critical line illustrates an important point: Mass extinctions need not be caused by disruptions of the carbon cycle (*2*).

Modern investigations of mass extinctions often emphasize a plurality of causes. Erwin's "complex web of causality" (*8*, *37*) addresses how a combination of volcanism, climate change, marine anoxia, methane release, and other environmental stressors may have contributed to the end-Permian extinction. Recent studies of the end-Cretaceous extinction consider massive volcanism (*38*) in addition to a bolide impact (*39*). Flood basalt eruptions are also clearly associated with the end-Triassic (*40*) and end-Permian (*15*) extinctions, but their contribution to CO_2 levels is ostensibly modest (*41*). Evidently, the carbon cycle both indicates and excites Earth system change. These dual roles merge, however, if external perturbations cause the cycle to respond by magnifying the initial disturbance. System-wide instability may then follow. Because the critical rate r_c bounds qualitatively different dynamical regimes, perturbations that exceed r_c (at time scales much greater than τ_x) suggest such unstable evolution. The carbon cycle thus becomes one of many environmental stressors, and an array of causes is naturally implicated.

Multiple causes may also be responsible for a "sixth extinction" (*1*, *42*). However, the anthropogenic disturbance of the carbon cycle merits its own appraisal. If an anomalous flux greater than M_c/τ_x brings the carbon cycle past a stability threshold at time scales much greater than $\tau_x \sim 10^4$ years, then the instantaneous addition of an anomalous mass greater than M_c will excite similar behavior. The existence of these thresholds is this paper's central hypothesis. If they exist, one would expect that an instability resulting from an impulsive addition of CO_2 would play out over a time scale with the same order of magnitude as the damping time scale τ_x. The upshot is that an unstable trajectory would reach its maximum extent roughly 10^4 years after the threshold is breached. But how that process plays out remains unknown.

MATERIALS AND METHODS

The event database

After a brief discussion of possible sources of error, this section summarizes how each event has been identified and quantified. Geological, paleoenvironmental, and paleobiological context is also given, as are relevant references. All data, including the identification of abbreviations, are provided in Table 1.

When multiple observations are used to compute a mean, the sample SD, the unaveraged observations, or both are noted in the event's description. However, these quantities only indicate the variability of a particular set of observations rather than an estimate of the observational error. As with any compilation of isotopic data [for example, Hayes *et al.* (*43*)], inadequate sampling may be a more significant problem. Here, it takes two forms: the sheer paucity of observations, and biases deriving from not only the original investigators—who may favor larger isotopic excursions—but also the needs of the present compilation, which favors carbon isotopic studies associated with strong geochronological constraints. An additional source of error derives from incompleteness of the sedimentary record. For example, a hiatus in sediment deposition, or erosion after deposition, may make the true carbon isotopic minimum effectively unavailable to the modern observer, thereby leading to an underestimate of $|\Delta_r|$.

The ideal geochronological control would provide absolute dates at the initiation and termination of isotopic excursions. Only one event in the database—at the Ediacaran-Cambrian boundary—meets this standard. Among the others, all but 1 of the 18 events extending from the Toarcian (182 Ma) to the Miocene (16 Ma) are timed by astrochronology, including, in some cases, information obtained from isotope geochronology. The duration of five of the older, pre-Jurassic events is determined from at least two dates provided by U-Pb geochronology that bracket less than twice the accumulation of sediment deriving from the event itself; a sixth event (end-Permian) comes close to this standard.

The remaining pre-Quaternary events are timed by biostratigraphy with reference to the Geologic Time Scale (*44*); their time scales are therefore the most poorly constrained. Two of them, the end-Ordovician and Frasnian-Famennian events, are among the Big Five mass extinctions. A third mass extinction—the end-Triassic—is constrained by both isotope geochronology and astrochronology, but these constraints are not directly associated with the carbonate–carbon isotope excursion.

If these three mass extinction events and the other four events with poor temporal constraints (Cambrian Spice, Tournaisian, mid-Capitanian, and Albian-Cenomanian) are removed from the database, the trends in Figs. 2 and 3 remain intact and no new trends appear.

Nevertheless, the unknown errors in the observations render quantitative error analysis infeasible. The representative error bars for Δ_r, M, and τ_{env} in Figs. 2 and 3 are instead guides for interpretation.

The following list proceeds from the oldest to the youngest event.

Ediacaran-Cambrian boundary, ~541 Ma

The magnitude and duration of this negative isotopic excursion derive from the Oman carbon isotope data of Amthor *et al.* (*45*) and the U-Pb geochronology of Bowring *et al.* (*46*). Other data from Morocco, Siberia, Mongolia, and China (*47*, *48*) suggest global consistency. The absence of the Ediacaran biota in the Cambrian has led to the suggestion that the Ediacaran biota vanished by mass extinction at the end of the Ediacaran, possibly related to the environmental event signaled by this excursion (*45*, *49*–*52*). However, gradual extinction coupled with permanent environmental changes unfavorable to preservation of the Ediacaran biota may also be possible (*53*).

Nemakit-Daldynian-Tommotian boundary, ~525 Ma

Both the carbon isotopic excursion and the U-Pb dates establishing the duration of this Early Cambrian event are from the Moroccan data of Maloof *et al.* (*47*, *54*); data from Siberia, Mongolia, and China confirm its global nature (*47*, *48*). No mass extinction has been associated with this interval. However, diversity (number of genera) and disparity (number of classes) sharply increase in the Tommotian, primarily because of the rise of small shelly fossils (*55*). The Nemakit-Daldynian-Tommotian boundary is also associated with a transition from seawater chemistry that favored aragonite precipitation to seawater favoring calcite precipitation (*47*, *56*).

Cambrian Spice, ~497 Ma

The duration and magnitude of this late Cambrian event, also known as the Steptoean positive carbon isotope excursion, are taken from the Australian data of Saltzman *et al.* (*57*). The event has also been found in North America, China, Kazakhstan, and Sweden (*58*, *59*). The initiation of this positive isotopic excursion coincides with an extinction of trilobites (*58*).

End-Ordovician event, ~446 Ma

The latest stage of the Ordovician—the Hirnantian—simultaneously exhibits a positive isotopic excursion and one of the Big Five mass extinctions. I estimated the magnitude of the negative limb of the excursion from data obtained at Vinni Creek and Monitor Range, Nevada (*60*), Copenhagen Canyon, Nevada (*61*), Blackstone Range, Yukon (*60*), Wangjiawan, south China (*62*), the Kardla drill core, Estonia (*63*), and Anticosti Island, Quebec (*64*). The seven data sets yield a mean excursion of 5.6 ± 0.9‰. Each data set except for Copenhagen Canyon has been correlated to graptolite zones by Gorjan *et al.* (*62*). By estimating the fraction of the *persculptus* and *extraordinarius* zones in which the excursion occurs at each site and estimating those time intervals from Gradstein *et al.* (*44*), I found that the negative limb of the excursion lasted approximately 230 ky.

Silurian Mulde event, ~428 Ma

A sequence of two positive excursions, known as the "Mulde event," occurs in the Homerian stage of the Silurian, during a period of graptolite extinctions known as the "Big Crisis" (*65*). The event is apparently global (*65*). Cramer *et al.* (*66*) have recently bracketed the earlier of the two excursions between two U-Pb dates obtained in Gotland, Sweden. I focused on the negative downswing, which occupies somewhat more than half of the dated interval, and estimated its duration to be about 260 ky. As shown by Cramer *et al.* (*66*), the Gotland excursion correlates well with observations in the West Midlands, England, with the West Midlands excursion having a magnitude of about 4‰ and the Gotland excursion about 2‰, a range that is consistent with other observations (*65*, *66*). I therefore estimated the magnitude to be 3 ± 1‰.

Silurian Lau event, ~423 Ma

A significant global positive carbon isotopic excursion known as the "Lau Event" occurs in the Ludlow Epoch of the Silurian (*65*, *67*–*72*). The excursion typically peaks at 6 to 8‰ [for example, Lehnert *et al.* (*71*)], though values as small as 3 to 4‰ and as high as 10 to 11‰ have been observed in North America (*68*) and Sweden (*70*), respectively. Given that uncertainty, I adopted a conservative mean peak value of 7‰. The negative downswing after the peak typically bottoms out at about 1‰, resulting in a typical total negative shift of about 6‰. Cramer *et al.* (*72*) have recently bracketed the duration of the excursion by U-Pb geochronology, finding that it must be less than about 1.17 My. Following their analysis, I took the upswing and downswing to be roughly symmetric, each occupying about one-half of an approximately million-year interval, implying that the duration of the downswing is about 500 ky.

Frasnian-Famennian boundary, ~372 Ma

The boundary between the Frasnian and Famennian stages in the Late Devonian is associated with one of the Big Five mass extinctions (*5*, *6*). But the drop in diversity at the boundary is thought to be a consequence of a lack of originations rather than an elevated extinction rate (*19*, *20*). The boundary is associated with a global positive carbon isotopic excursion, known as the Upper Kellwasser Event (*73*). The magnitude and duration of the excursion are taken from the compilation of European Devonian data of Buggisch and Joachimski (*74*).

Tournaisian event, ~352 Ma

Buggisch *et al.* (*75*) presented carbon isotopic data from Belgium, Ireland, France, western Canada, and the western United States that collectively exhibit a pronounced positive isotopic excursion in the Tournaisian stage of the Carboniferous. Using their biostratigraphic time scale, I estimated the duration of the negative limb of the excursion to be 1.51 My; the magnitude of the excursion in their compilation is about 3.5‰.

Mid-Capitanian event, ~262 Ma

A mass extinction in the Capitanian Stage of the Middle Permian is associated with a negative isotopic excursion of carbonate carbon of about 5‰ over about 500 ky (*76*, *77*). Observations of the event in south China suggest that the extinction event coincides with the initiation of Emeishan volcanism (*78*) and the onset of the excursion (*76*).

End-Permian extinction, ~252 Ma

The end-Permian extinction is considered the most severe of the Big Five (*8*). A significant negative isotopic excursion occurs at the time of the extinction, just below the Permian-Triassic boundary. Korte and Kozur (*16*) reviewed observations of the excursion in 40 localities worldwide and concluded that the excursion ranged from 4 to 7‰; I therefore took the magnitude of the excursion to be at the center of that distribution (5.5‰). The 60-ky duration of the excursion derives from the well-studied section at Meishan, south China, where Cao *et al.* (*79*) have provided high-resolution carbon isotopic data and U-Pb geochronology provides strong constraints on the time scale (*9*).

Early Triassic, ~251 Ma

Several significant isotopic excursions of unknown origin follow the end-Permian extinction (*80*–*83*). Galfetti *et al.* (*83*) provided carbon isotopic data tied to U-Pb geochronology from the Loulou Formation, northwest Guanxi, south China. The only temporally constrained

negative isotopic shift occurs in a negative excursion that begins approximately 251.22 Ma (*83*) in the mid-Smithian and declines approximately 3.5‰ over approximately 250 ky.

Triassic-Jurassic boundary, ~201 Ma

One of the Big Five extinctions, the end-Triassic event is temporally associated with the emplacement of the Central Atlantic magmatic province (*40*). Geochemically, the most well-studied section is at St. Audries Bay in southwest England, where the extinction interval coincides with a rapid fall and subsequent rise of the isotopic composition of organic matter (*84*) that lasts 20 to 40 ky according to astrochronology (*85*). This so-called initial excursion in organic carbon is widely observed (*86*). However, its significance for understanding the evolution of marine dissolved inorganic carbon is unclear (*86*, *87*), partly because it may be associated with observed changes in flora (*87*)—and therefore variations in the organic matter itself—and partly because inorganic isotopic compositions need not track organic isotopic compositions (*43*). There are unfortunately few well-resolved isotopic studies of carbonate carbon associated with the end-Triassic event (*88*–*93*). These carbonate studies also reveal a negative excursion associated with the extinction, but it is often unclear if they represent the "initial excursion" or the later 120-ky-long "main excursion" seen in organic carbon (*84*, *85*). A recent review (*94*) cautions that diagenetic alteration may have corrupted carbonate data, yet a careful study of lithological effects at an Italian section suggests that the carbonate excursion may indeed be primary (*87*). An important additional problem is the need to estimate the time scale of the carbonate excursion. The data of Clémence *et al.* (*92*) provide a solution to these problems. In their analysis of inorganic and organic carbonate at the Tiefengraben section in the Austrian Alps, they found an initial 2‰ negative excursion in carbonate that extended to the second significant minimum in their organic data (*92*), which in turn correlates reasonably well with the astrochronologically calibrated organic data at St. Audries Bay (*85*). Their initial carbonate excursion was then found to last approximately 50 ky [which included one precessional cycle of the "pre-recovery" interval identified by Ruhl *et al.* (*85*)]. This 2.0‰ shift is also consistent with isotopic analyses of carbonate in pristine oysters located near St. Audries Bay (*91*).

Toarcian oceanic anoxic event, ~183 Ma

The early Toarcian oceanic anoxic event (*95*) is widely observed in Europe as a negative excursion in the isotopic composition of carbonate (*96*–*99*). To estimate its magnitude and duration, I used the high-resolution carbonate record of Hesselbo *et al.* (*96*) obtained at Peniche (Portugal). The astrochronology of Suan *et al.* (*97*) found a duration of 150 ky (their interval C1) for the negative isotopic excursion, which is consistent with the subsequent analysis of Huang and Hesselbo (*100*). Using this chronology, recent U-Pb dating by Burgess *et al.* (*101*) found that the intrusive magmatism associated with the Ferrar large igneous province is synchronous with the negative excursion.

Aptian oceanic anoxic event, ~120 Ma

The negative isotopic excursion associated with the Aptian oceanic anoxic event has been observed worldwide in open ocean records of carbonate carbon (*102*–*105*). My estimate of the magnitude and duration of the excursion derived from the astrochronology of Malinverno *et al.* (*106*) performed on the carbonate record of Erba *et al.* (*103*). The negative excursion spans the interval C3 [originally identified by Menegatti *et al.* (*102*)] and lasts approximately 47 ky.

Albian-Cenomanian boundary, ~100 Ma

This complex carbon isotope event occurred near the Albian-Cenomanian boundary (mid-Cretaceous) in several European sections (*107*). Here, I focused on the carbon isotopic data obtained at Ocean Drilling Program (ODP) Site 1050 at Blake Nose, western North Atlantic, as presented by Ando *et al.* (*108*). When plotted using the time scale of Huber *et al.* (*109*), the ODP data show an unambiguous 0.7‰ negative excursion across the boundary over approximately 110 ky.

Mid-Cenomanian event, ~95.9 Ma

The mid-Cenomanian positive carbon isotopic excursion has been clearly observed in European sections (*107*), the North Atlantic (*110*), western North America (*111*), and elsewhere. My analysis follows from the correlation of the "English Chalk" reference carbonate curve (*107*) to carbon isotopic data from the Cretaceous Western Interior Seaway of North America (*111*, *112*). I used the time scale of Eldrett *et al.* (*112*), which is based on a combination of astrochronology and U-Pb geochronology. As indicated in figure 11 of Eldrett *et al.* (*112*), the negative swing of the excursion begins at about 96.5 Ma, followed by a decline of about 0.85‰ over roughly 138 ky.

Cenomanian-Turonian boundary event, ~94.2 Ma

Otherwise known as oceanic anoxic event 2, the positive isotopic excursion at the Cenomanian-Turonian boundary is probably the most widely observed of the Cretaceous isotopic events (*107*, *111*, *112*). As for the mid-Cenomanian event, my estimate of the time scale and magnitude of the Cenomanian-Turonian event follows from the correlation of the English Chalk reference carbonate curve (*107*) to carbon isotopic data from the Cretaceous Western Interior Seaway of North America (*111*, *112*). I took the initiation of the event to be at the positive peak labeled B in figure 11 of Eldrett *et al.* (*112*) and found that the ensuing negative excursion declines by 1.60‰ in roughly 553 ky.

Cretaceous-Paleogene extinction, ~65.5 Ma

The end-Cretaceous negative isotopic excursion is associated with one of the Big Five extinctions (*5*), widely known for the extinction of dinosaurs and the Alvarez impact hypothesis (*39*). Its temporal association with the eruption of the massive Deccan volcanic province in India is less widely known (*38*). I obtained the magnitude and time scale of the carbon isotopic event from the deep-sea bulk carbon isotopic data obtained at ODP Sites 1210 (Northwest Pacific) and 1262 (South Atlantic), as presented by Alegret *et al.* (*113*) using an orbitally tuned time scale (*114*). I took the initiation and termination of the approximately 1.15 ± 0.03‰ (the mean of 1.16 and 1.13‰) negative isotopic excursion at each site to be where values of δ_1 begin to change by at least 0.1‰, resulting in a mean event duration of roughly 26 ky (the average of 8.5 and 44 ky).

Early late Paleocene event, ~58.9 Ma

Also known as the mid-Paleocene biotic event, this negative excursion is synchronous with dissolution of carbonate and changes in the organization of benthic and planktonic ecosystems (*115*, *116*). The magnitude and time scale of this negative excursion are taken from the high-resolution bulk isotopic record of Littler *et al.* (*115*).

Paleocene-Eocene Thermal Maximum, ~55.5 Ma

The negative isotopic excursion of the Paleocene-Eocene Thermal Maximum is perhaps the most studied carbon isotopic event in Earth history (*11*), in large part because of its association with significant climate warming and clear evidence of ocean acidification (*10*). The event is also associated with a significant extinction of benthic foraminifera (*12*); however, other groups of benthic and planktic microfossils show little or no extinction (*11*). The time scales of the isotopic excursion of bulk carbonate in two deep-sea cores, from ODP Site 1266 on the Walvis Ridge in the South Atlantic and ODP Site 690 in the Weddell Sea, Southern Ocean, have each been estimated independently by identification of orbital cycles (*117*) and the estimation of sedimentation rates

from the concentration of ^{3}He (*118*, *119*). The mean of the resulting four estimates [corresponding to the cumulative time between the onset of the excursion and the termination of its "core" as summarized in table 1 of Murphy *et al.* (*119*)] is 83 ± 23 ky. I obtained the magnitude of the isotopic excursion, 2.7 ± 1.1‰, from the mean of 33 published analyses of bulk Paleocene-Eocene Thermal Maximum carbonates reviewed by McInerney and Wing (*11*). The initial value of the excursion was obtained similarly (*11*). Although these averages lack prejudice, they may nevertheless underestimate the excursion's size (*120*) and overestimate its time scale (*121*).

Eocene Thermal Maximum 2, ~53.7 Ma

The Eocene is punctuated by several "hyperthermal events," each represented by a negative excursion in the isotopic composition of carbonate carbon and dissolution of deep-sea marine carbonates. Eocene Thermal Maximum 2, one such event, follows the Paleocene-Eocene Thermal Maximum (also known as Eocene Thermal Maximum 1) by roughly 2 My. My estimate of the magnitude of Eocene Thermal Maximum 2 derived from averaging estimates from four high-resolution bulk isotopic records presented by Stap *et al.* (*122*). The records derive from ODP Sites 1262, 1263, 1265, and 1267, corresponding to paleowater depths ranging from about 1500 to 3600 m (*122*); the shallowest site yields an excursion of about 1.5‰, whereas the others are each about 1.0‰ (*122*), yielding a mean of 1.13 ± 0.25‰. The time scale is about 45 ky.

Eocene Hyperthermal H2, ~53.6 Ma

The magnitude and time scale of this Eocene hyperthermal event come from ODP Sites 1263, 1265, and 1267. Following Stap *et al.* (*122*), I took the excursion of bulk carbon isotopes to be about 0.6‰ and the time scale to be about 33 ky.

Eocene Hyperthermal I1, ~53.2 Ma

I obtained the magnitude (0.72‰) and time scale (41 ky) of this Eocene hyperthermal event from the high-resolution bulk carbon isotopic record of Littler *et al.* (*115*), which derives from ODP Site 1262.

Eocene Hyperthermal I2, ~53.1 Ma

This Eocene hyperthermal follows Eocene Hyperthermal I1 by about 100 ky. Using the same source (*115*) as for Eocene Hyperthermal I1, I found an excursion of about 0.61‰ and a time scale of 40 ky.

Eocene Thermal Maximum 3, ~52.5 Ma

I estimated the magnitude and time scale of this hyperthermal event from the high-resolution benthic carbon isotopic record of Lauretano *et al.* (*123*), obtained at ODP Sites 1262 and 1263. The two records are similar, yielding an excursion of about 0.8‰ and a time scale of about 37 ky.

Early Oligocene Event, ~33.5 Ma

The positive carbon isotopic excursion just above the Eocene-Oligocene boundary is associated with the initiation of permanent Cenozoic ice sheets on Antarctica (*124*–*126*). I focused on the negative downswing to lighter isotopic compositions that followed. The time scale and isotopic change are derived from the high-resolution data collected at ODP Site 1218, using the astrochronological time scale presented by Coxall *et al.* (*125*). The negative shift extends over roughly 0.6 ± 0.1‰ during a period of about 430 ± 100 ky. The three ODP records presented by Zachos and Kump (*126*) are consistent with these estimates.

Miocene Climatic Optimum 1, ~16.9 Ma

Holbourn *et al.* (*127*) provided high-resolution carbon isotopic records spanning most of the Miocene Climatic Optimum, a period of warm climates ranging from 17.0 to 14.7 Ma that interrupted the longer-term trend of Cenozoic cooling. The records are obtained from Integrated ODP Site U1337 in the eastern equatorial Pacific Ocean, at a paleowater depth of 3500 to 4000 m. The Miocene Climatic Optimum began with a negative isotopic excursion, which I designated Miocene Climatic Optimum 1, that has also been identified in lower-resolution records from three other sites, elsewhere in the Pacific and in the Southern Ocean (*127*). I obtained the magnitude (0.5‰) and time scale (28 ky) from the bulk carbonate record. The event is synchronous with shoaling of the carbonate compensation depth (CCD).

Miocene Climatic Optimum 2, ~16.4 Ma

Holbourn *et al.* (*127*) identified three other Miocene Climatic Optimum negative excursions, which I designated Miocene Climatic Optimum 2 to Miocene Climatic Optimum 4, during which δ_1 decreases sharply and the CCD appears to shoal. Using the same high-resolution record as for Miocene Climatic Optimum 1, I found that Miocene Climatic Optimum 2 has a time scale of 22 ky and a magnitude of 0.76‰.

Miocene Climatic Optimum 3, ~16.0 Ma

See Miocene Climatic Optimum 2. For Miocene Climatic Optimum 3, I found a time scale of 32 ky and a magnitude of 0.66‰. This event also appears in the records of ODP Site 1146 in the western Pacific Ocean (*128*) and ODP Site U1338 in the eastern equatorial Pacific (*129*).

Miocene Climatic Optimum 4, ~15.6 Ma

See Miocene Climatic Optimum 2. For Miocene Climatic Optimum 4, the excursion has a magnitude of 0.6‰ and a time scale of 29 ky.

Last Glacial Maximum–to–Holocene deglacial, ~0.021 Ma

Using a compilation of 480 records of benthic foraminiferal carbon isotope analyses, Peterson *et al.* (*130*) estimated a whole-ocean increase in the isotopic composition of dissolved inorganic carbon of 0.34 ± 0.19‰ from the Last Glacial Maximum to the Holocene. I took the time scale to be 18 ky, given their Last Glacial Maximum averages over 19 to 23 ky and Holocene averages over 0 to 6 ky. This is the only positive isotopic shift in the database in which the magnitude and time scale derive from the upswing; for the others, such as the Ordovician, the calculations correspond to the ensuing downshift.

The boundary value problem

The boundary value problem derives from a model of the global carbon isotopic system presented by Rothman *et al.* (*131*, *132*). This model partitions carbon into two reservoirs. The inorganic reservoir contains a mass m of carbon with isotopic composition δ_1; the organic reservoir contains carbon of isotopic composition δ_2. In the Phanerozoic, the isotopic composition of the organic reservoir typically equilibrates with respect to inputs and outputs at time scales much faster than the inorganic reservoir (*131*). The evolution of δ_1 is then described by equation 8 of Rothman *et al.* (*132*):

$$m\frac{d\delta_1}{dt} = j_i(\delta_i - \delta_1) + b_2\varepsilon \tag{8}$$

where j_i is the flux of carbon of isotopic composition δ_i into the surface carbon cycle (deriving typically from volcanism and continental weathering), b_2 is the burial flux of organic carbon out of the surface cycle, and $\varepsilon = \delta_1 - \delta_2$ is the isotopic fractionation between inorganic and organic carbon.

Suppose now that a new source of carbon with isotopic composition δ_i' flows into the carbon cycle with flux j_i', and that the burial flux b_2 increases by an amount b_2' while ε remains constant. Equation 8 then becomes

$$m\frac{d\delta_1}{dt} = j_i^*(\delta_i^* - \delta_1) + j_i'(\delta_i' - \delta_1) + (b_2^* + b_2')\varepsilon \tag{9}$$

where j_i^*, δ_i^*, and b_2^* represent unperturbed quantities that satisfy the steady-state relation

$$0 = j_i^*(\delta_i^* - \delta_1^*) + b_2^*\varepsilon \tag{10}$$

where δ_1^* is the steady-state isotopic composition of the inorganic reservoir. Subtraction of Eq. 10 from Eq. 9 then yields

$$m\frac{d\delta_1}{dt} = -j_i^*(\delta_1 - \delta_1^*) + j_i'(\delta_i' - \delta_1) + b_2'\varepsilon \tag{11}$$

Here, δ_i' is set to the average isotopic composition of Phanerozoic organic carbon (−27.8‰ (*21*)]. Consequently, the terms in Eq. 11 proportional to j_i' and b_2' are practically indistinguishable so that a positive perturbation of the input flux is equivalent to a negative perturbation of the burial flux. I therefore set $b_2' = 0$ and reinterpreted j_i' as representative of any perturbation of the flux to the inorganic reservoir that carries the isotopic composition of organic matter.

Further simplifications follow by reexpressing the remaining terms in Eq. 11 using variables defined in the main text. First, recall that the mass m is decomposed into an unperturbed component m^* and a perturbation Δm according to

$$m(t) = m^* + \Delta m(t) \tag{12}$$

where, by definition,

$$\Delta m(t) = \int_0^t j_i'(t')dt' \tag{13}$$

Substitution of Eq. 12 into Eq. 9 and division of both sides by m^* then yields, for $b_2' = 0$

$$\left(1 + \frac{\Delta m}{m^*}\right)\frac{d\delta_1}{dt} = -\frac{j_i^*}{m^*}(\delta_1 - \delta_1^*) + \frac{j_i'}{m^*}(\delta_i' - \delta_1) \tag{14}$$

Recall also the definitions of the normalized mass perturbation

$$M = \Delta m/m^* \tag{15}$$

the normalized input flux

$$J = j_i'/j_i^* \tag{16}$$

and the turnover time

$$\tau_0 = m^*/j_i^* \tag{17}$$

Inserting each of these expressions into Eq. 14, one obtains

$$\frac{d\delta_1}{dt} = \frac{1}{\tau_0(1+M)}\left[-(\delta_1 - \delta_1^*) + J(\delta_i' - \delta_1)\right] \tag{18}$$

The normalized mass perturbation evolves as

$$\frac{dM}{dt} = J/\tau_0 \tag{19}$$

which is obtained by taking the derivative of both sides of Eq. 13 and using Eqs. 15 to 17. Finally, the derivative of Eq. 4 in the main text provides the evolution of the normalized flux perturbation

$$\frac{dJ}{dt} = \phi/\tau_{env} \tag{20}$$

The differential equations 18 to 20 describe changes in the isotopic composition of marine inorganic carbon in response to the normalized flux $J(t)$. The first term in parentheses in Eq. 18 encodes the tendency of δ_1 to relax back to the initial value δ_1^*, and the second term describes the forcing of the system out of steady state by injection of carbon with isotopic composition δ_i'. Because ϕ is unknown, the solution of this system requires not only three initial conditions but also one end condition:

$$\delta_1(0) = \delta_1^* \tag{21}$$

$$M(0) = 0 \tag{22}$$

$$J(0) = 0 \tag{23}$$

$$_{\delta 1}(\tau_{env}) = \delta_1^* + \Delta_r \tag{24}$$

Equations 18 to 24 constitute the complete boundary value problem. The solution for ϕ, which is obtained numerically, provides the evolution of $\delta_1(t)$ that matches its observed initial and final states while remaining consistent with Eqs. 18 to 20.

Turnover time, the organic burial fraction, and ϕ_c

Equation 17 shows that the turnover time τ_0 equals the mass m^* of inorganic carbon in the oceans divided by the input flux j_i^*. In steady state, the latter is equal to the rate at which carbon is immobilized in marine sediments. The modern preindustrial reservoir of dissolved inorganic carbon is about 38,000 Pg (*133*). Sedimentary organic carbon and carbonate carbon are immobilized in sediments at the total preindustrial rate of approximately 0.28 Pg year^{-1} (*134*, *135*). By dividing the reservoir size by the sequestration rate, one obtains $\tau_0 \simeq 140$ ky.

Krissansen-Totton *et al.* (*21*) have recently provided a comprehensive analysis of the evolution of the organic burial fraction through geologic time, commonly designated as f. Their study of the Phanerozoic portion of the record largely derives from an earlier analysis of Hayes *et al.* (*43*); both studies find $f \simeq 0.23$, which this paper assigns to ϕ_c. Hayes *et al.* (*43*) compute f in a series of contiguous intervals throughout the Phanerozoic, obtaining a sequence f_i. The root mean square (rms) fluctuation of the f_i's is 0.037. The error assigned to ϕ_c is twice the rms fluctuation.

REFERENCES AND NOTES

1. A. D. Barnosky, N. Matzke, S. Tomiya, G. O. U. Wogan, B. Swartz, T. B. Quental, C. Marshall, J. L. McGuire, E. L. Lindsey, K. C. Maguire, B. Mersey, E. A. Ferrer, Has the Earth's sixth mass extinction already arrived? *Nature* **471**, 51–57 (2011).

2. A. Hallam, P. B. Wignall, *Mass Extinctions and Their Aftermath* (Oxford Univ. Press, 1997).
3. S. M. Stanley, Relation of Phanerozoic stable isotope excursions to climate, bacterial metabolism, and major extinctions. *Proc. Natl. Acad. Sci. U.S.A.* **107**, 19185–19189 (2010).
4. O. H. Walliser, *Global Events and Event Stratigraphy in the Phanerozoic* (Springer, 1996).
5. D. M. Raup, Biological extinction in Earth history. *Science* **231**, 1528–1533 (1986).
6. R. K. Bambach, Phanerozoic biodiversity mass extinctions. *Annu. Rev. Earth Planet. Sci.* **34**, 127–155 (2006).
7. J. Alroy, Accurate and precise estimates of origination and extinction rates. *Paleobiology* **40**, 374–397 (2014).
8. D. H. Erwin, *Extinction: How Life on Earth Nearly Ended 250 Million Years Ago* (Princeton Univ. Press, 2006).
9. S. D. Burgess, S. Bowring, S.-z. Shen, High-precision timeline for Earth's most severe extinction. *Proc. Natl. Acad. Sci. U.S.A.* **111**, 3316–3321 (2014).
10. J. C. Zachos, U. Röhl, S. A. Schellenberg, A. Sluijs, D. A. Hodell, D. C. Kelly, E. Thomas, M. Nicolo, I. Raffi, L. J. Lourens, H. McCarren, D. Kroon, Rapid acidification of the ocean during the Paleocene-Eocene thermal maximum. *Science* **308**, 1611–1615 (2005).
11. F. A. McInerney, S. L. Wing, The Paleocene-Eocene Thermal Maximum: A perturbation of carbon cycle, climate, and biosphere with implications for the future. *Annu. Rev. Earth Planet. Sci.* **39**, 489–516 (2011).
12. E. Thomas, N. J. Shackleton, The Paleocene-Eocene benthic foraminiferal extinction and stable isotope anomalies. *Geol. Soc. Lond. Spec. Publ.* **101**, 401–441 (1996).
13. R. P. Speijer, C. Scheibner, P. Stassen, A.-M. M. Morsi, Response of marine ecosystems to deep-time global warming: A synthesis of biotic patterns across the Paleocene-Eocene thermal maximum (PETM). *Aust. J. Earth Sci.* **105**, 6–16 (2012).
14. R. D. Norris, S. K. Turner, P. M. Hull, A. Ridgwell, Marine ecosystem responses to Cenozoic global change. *Science* **341**, 492–498 (2013).
15. S. D. Burgess, S. A. Bowring, High-precision geochronology confirms voluminous magmatism before, during, and after Earth's most severe extinction. *Sci. Adv.* **1**, e1500470 (2015).
16. C. Korte, H. W. Kozur, Carbon-isotope stratigraphy across the Permian–Triassic boundary: A review. *J. Asian Earth Sci.* **39**, 215–235 (2010).
17. M. J. S. Rudwick, *Georges Cuvier, Fossil Bones, and Geological Catastrophes* (University of Chicago Press, 1997).
18. N. D. Newell, Crises in the history of life. *Sci. Am.* **208**, 76–93 (1963).
19. G. R. McGhee Jr., The late Devonian extinction event: Evidence for abrupt ecosystem collapse. *Paleobiology* **14**, 250–257 (1988).
20. R. K. Bambach, A. H. Knoll, S. C. Wang, Origination, extinction, and mass depletions of marine diversity. *Paleobiology* **30**, 522–542 (2004).
21. J. Krissansen-Totton, R. Buick, D. C. Catling, A statistical analysis of the carbon isotope record from the Archean to Phanerozoic and implications for the rise of oxygen. *Am. J. Sci.* **315**, 275–316 (2015).
22. E. T. Sundquist, Influence of deep-sea benthic processes on atmospheric CO_2. *Philos. Trans. R. Soc. Lond. A Math. Phys. Eng. Sci.* **331**, 155–165 (1990).
23. D. Archer, H. Kheshgi, E. Maier-Reimer, Dynamics of fossil fuel CO_2 neutralization by marine $CaCO_3$. *Global Biogeochem. Cycles* **12**, 259–276 (1998).
24. D. Archer, Fate of fossil fuel CO_2 in geologic time. *J. Geophys. Res.* **110**, C09S05 (2005).
25. A. Ridgwell, J. C. Hargreaves, Regulation of atmospheric CO_2 by deep-sea sediments in an Earth system model. *Global Biogeochem. Cycles* **21**, GB2008 (2007).
26. A. Ridgwell, A Mid Mesozoic Revolution in the regulation of ocean chemistry. *Mar. Geol.* **217**, 339–357 (2005).
27. A. Ridgwell, R. E. Zeebe, The role of the global carbonate cycle in the regulation and evolution of the Earth system. *Earth Planet. Sci. Lett.* **234**, 299–315 (2005).
28. P. R. Bown, J. A. Lees, J. R. Young, Calcareous nannoplankton evolution and diversity through time, in *Coccolithophores—From Molecular Processes to Global Impact*, H. R. Thierstein, J. R. Young, Eds. (Springer, 2004), pp. 481–508.
29. C. de Vargas, M.-P. Aubry, I. Probert, J. Young, Origin and evolution of coccolithophores: From coastal hunters to oceanic farmers, in *Evolution of Primary Producers in the Sea*, P. G. Falkowski, A. H. Knoll, Eds. (Elsevier, 2007), vol. 12, pp. 251–285.
30. R. E. Zeebe, P. Westbroek, A simple model for the $CaCO_3$ saturation state of the ocean: The "Strangelove," the "Neritan," and the "Cretan" Ocean. *Geochem. Geophys. Geosyst.* **4**, 1104 (2003).
31. J. L. Sarmiento, N. Gruber, *Ocean Biogeochemical Dynamics* (Princeton Univ. Press, 2006).
32. D. Archer, *The Global Carbon Cycle* (Princeton Univ. Press, 2010).
33. M. R. Saltzman, E. Thomas, Carbon isotope stratigraphy, in *The Geologic Time Scale*, F. M. Gradstein, J. G. Ogg, M. Schmitz, Eds. (Elsevier, 2012), vol. 1, pp. 207–232.
34. P. Ciais, C. Sabine, G. Bala, L. Bopp, V. Brovkin, J. Canadell, A. Chhabra, R. DeFries, J. Galloway, M. Heimann, C. Jones, C. Le Quéré, R. B. Myneni, S. Piao, P. Thornton, Carbon and other biogeochemical cycles, in *Climate Change 2013: The Physical Science Basis. Contribution of Working Group I to the Fifth Assessment Report of the Intergovernmental Panel on Climate Change*, T. F. Stocker, D. Qin, G.-K. Plattner, M. Tignor, S. K. Allen, J. Boschung, A. Nauels, Y. Xia, V. Bex, P. M. Midgley, Eds. (Cambridge Univ. Press, 2013), pp. 465–570.
35. D. P. van Vuuren, J. Edmonds, M. Kainuma, K. Riahi, A. Thomson, K. Hibbard, G. C. Hurtt, T. Kram, V. Krey, J.-F. Lamarque, T. Masui, M. Meinshausen, N. Nakicenovic, S. J. Smith, S. K. Rose, The representative concentration pathways: An overview. *Clim. Change* **109**, 5–31 (2011).
36. G. R. Dickens, J. R. O'Neil, D. K. Rea, R. M. Owen, Dissociation of oceanic methane hydrate as a cause of the carbon isotope excursion at the end of the Paleocene. *Paleoceanography* **10**, 965–971 (1995).
37. D. H. Erwin, The Permo–Triassic extinction. *Nature* **367**, 231–236 (1994).
38. B. Schoene, K. M. Samperton, M. P. Eddy, G. Keller, T. Adatte, S. A. Bowring, S. F. R. Khadri, B. Gertsch, U-Pb geochronology of the Deccan Traps and relation to the end-Cretaceous mass extinction. *Science* **347**, 182–184 (2015).
39. L. W. Alvarez, W. Alvarez, F. Asaro, H. V. Michel, Extraterrestrial cause of the Cretaceous-Tertiary extinctions. *Science* **208**, 1095–1108 (1980).
40. T. J. Blackburn, P. E. Olsen, S. A. Bowring, N. M. McLean, D. V. Kent, J. Puffer, G. McHone, E. T. Rasbury, M. Et-Touhami, Zircon U-Pb geochronology links the end-Triassic extinction with the Central Atlantic Magmatic Province. *Science* **340**, 941–945 (2013).
41. S. Self, T. Thordarson, M. Widdowson, Gas fluxes from flood basalt eruptions. *Elements* **1**, 283–287 (2005).
42. E. Kolbert, *The Sixth Extinction: An Unnatural History* (Henry Holt and Company, 2014).
43. J. M. Hayes, H. Strauss, A. J. Kaufman, The abundance of ^{13}C in marine organic matter and isotopic fractionation in the global biogeochemical cycle of carbon during the past 800 Ma. *Chem. Geol.* **161**, 103–125 (1999).
44. F. M. Gradstein, J. G. Ogg, M. Schmitz, G. M. Ong, Eds., *The Geologic Time Scale 2012* (Elsevier, 2012), vol. 2.
45. J. E. Amthor, J. P. Grotzinger, S. Schröder, S. A. Bowring, J. Ramezani, M. W. Martin, A. Matter, Extinction of Cloudina and Namacalathus at the Precambrian-Cambrian boundary in Oman. *Geology* **31**, 431–434 (2003).
46. S. A. Bowring, J. P. Grotzinger, D. J. Condon, J. Ramezani, M. J. Newall, P. A. Allen, Geochronologic constraints on the chronostratigraphic framework of the Neoproterozoic Huqf Supergroup, Sultanate of Oman. *Am. J. Sci.* **307**, 1097–1145 (2007).
47. A. C. Maloof, S. M. Porter, J. L. Moore, F. Ö. Dudás, S. A. Bowring, J. A. Higgins, D. A. Fike, M. P. Eddy, The earliest Cambrian record of animals and ocean geochemical change. *Geol. Soc. Am. Bull.* **122**, 1731–1774 (2010).
48. E. F. Smith, F. A. Macdonald, T. A. Petach, U. Bold, D. P. Schrag, Integrated stratigraphic, geochemical, and paleontological late Ediacaran to early Cambrian records from southwestern Mongolia. *Geol. Soc. Am. Bull.* **128**, 442–468 (2016).
49. A. Seilacher, Late Precambrian and early Cambrian metazoa: Preservational or real extinctions?, in *Patterns of Change in Earth Evolution*, H. D. Holland, A. F. Trendall, Eds. (Springer, 1984), pp. 159–168.
50. M. D. Brasier, On mass extinction and faunal turnover near the end of the Precambrian, in *Mass Extinctions, Processes, and Evidence*, S. K. Donovan, Ed. (Columbia Univ. Press, 1989), pp. 73–88.
51. J. K. Bartley, M. C. Pope, A. H. Knoll, M. A. Semikhatov, P. Petrov, A Vendian-Cambrian boundary succession from the northwestern margin of the Siberian Platform: Stratigraphy, palaeontology, chemostratigraphy and correlation. *Geol. Mag.* **135**, 473–494 (1998).
52. A. H. Knoll, S. B. Carroll, Early animal evolution: Emerging views from comparative biology and geology. *Science* **284**, 2129–2137 (1999).
53. M. Laflamme, S. A. F. Darroch, S. M. Tweedt, K. J. Peterson, D. H. Erwin, The end of the Ediacara biota: Extinction, biotic replacement, or Cheshire Cat? *Gondw. Res.* **23**, 558–573 (2013).
54. A. C. Maloof, J. Ramezani, S. A. Bowring, D. A. Fike, S. M. Porter, M. Mazouad, Constraints on early Cambrian carbon cycling from the duration of the Nemakit-Daldynian–Tommotian boundary δ13C shift, Morocco. *Geology* **38**, 623–626 (2010).
55. C. R. Marshall, Explaining the Cambrian "explosion" of animals. *Annu. Rev. Earth Planet. Sci.* **34**, 355–384 (2006).
56. S. M. Porter, Seawater chemistry and early carbonate biomineralization. *Science* **316**, 1302 (2007).
57. M. R. Saltzman, S. A. Young, L. R. Kump, B. C. Gill, T. W. Lyons, B. Runnegar, Pulse of atmospheric oxygen during the late Cambrian. *Proc. Natl. Acad. Sci. U.S.A.* **108**, 3876–3881 (2011).
58. M. R. Saltzman, R. L. Ripperdan, M. D. Brasier, K. C. Lohmann, R. A. Robison, W. T. Chang, S. Peng, E. K. Ergaliev, B. Runnegar, A global carbon isotope excursion (SPICE) during the Late Cambrian: Relation to trilobite extinctions, organic-matter burial and sea level. *Palaeogeogr. Palaeoclimatol. Palaeoecol.* **162**, 211–223 (2000).
59. B. C. Gill, T. W. Lyons, S. A. Young, L. R. Kump, A. H. Knoll, M. R. Saltzman, Geochemical evidence for widespread euxinia in the Later Cambrian ocean. *Nature* **469**, 80–83 (2011).
60. D. F. LaPorte, C. Holmden, W. P. Patterson, J. D. Loxton, M. Melchin, C. E. Mitchell, S. C. Finney, H. D. Sheets, Local and global perspectives on carbon and nitrogen cycling

during the Hirnantian glaciation. *Palaeogeogr. Palaeoclimatol. Palaeoecol.* **276**, 182–195 (2009).
61. L. R. Kump, M. A. Arthur, M. E. Patzkowsky, M. T. Gibbs, D. S. Pinkus, P. M. Sheehan, A weathering hypothesis for glaciation at high atmospheric pCO_2 during the Late Ordovician. *Palaeogeogr. Palaeoclimatol. Palaeoecol.* **152**, 173–187 (1999).
62. P. Gorjan, K. Kaiho, D. A. Fike, C. Xu, Carbon-and sulfur-isotope geochemistry of the Hirnantian (Late Ordovician) Wangjiawan (Riverside) section, South China: Global correlation and environmental event interpretation. *Palaeogeogr. Palaeoclimatol. Palaeoecol.* **337–338**, 14–22 (2012).
63. S. A. Young, M. R. Saltzman, W. I. Ausich, A. Desrochers, D. Kaljo, Did changes in atmospheric CO_2 coincide with latest Ordovician glacial–interglacial cycles? *Palaeogeogr. Palaeoclimatol. Palaeoecol.* **296**, 376–388 (2010).
64. D. S. Jones, D. A. Fike, S. Finnegan, W. W. Fischer, D. P. Schrag, D. McCay, Terminal Ordovician carbon isotope stratigraphy and glacioeustatic sea-level change across Anticosti Island (Québec, Canada). *Geol. Soc. Am. Bull.* **123**, 1645–1664 (2011).
65. M. Calner, Silurian global events—At the tipping point of climate change, in *Mass Extinction*, A. M. T. Elewa, Ed. (Springer, 2008), pp. 21–57.
66. B. D. Cramer, D. J. Condon, U. Söderlund, C. Marshall, G. J. Worton, A. T. Thomas, M. Calner, D. C. Ray, V. Perrier, I. Boomer, P. J. Patchett, L. Jeppsson, U-Pb (zircon) age constraints on the timing and duration of Wenlock (Silurian) paleocommunity collapse and recovery during the "Big Crisis". *Geol. Soc. Am. Bull.* **124**, 1841–1857 (2012).
67. J. Wigforss-Lange, Carbon isotope ^{13}C enrichment in Upper Silurian (Whitcliffian) marine calcareous rocks in Scania, Sweden. *GFF* **121**, 273–279 (1999).
68. M. R. Saltzman, Silurian $\delta^{13}C$ stratigraphy: A view from North America. *Geology* **29**, 671–674 (2001).
69. D. Kaljo, V. Grytsenko, T. Martma, M.-A. Mõtus, Three global carbon isotope shifts in the Silurian of Podolia (Ukraine): Stratigraphical implications. *Est. J. Earth Sci.* **56**, 205–220 (2007).
70. L. Jeppsson, J. A. Talent, R. Mawson, A. J. Simpson, A. S. Andrew, M. Calner, D. J. Whitford, J. A. Trotter, O. Sandström, H.-J. Caldon, High-resolution Late Silurian correlations between Gotland, Sweden, and the Broken River region, NE Australia: Lithologies, conodonts and isotopes. *Palaeogeogr. Palaeoclimatol. Palaeoecol.* **245**, 115–137 (2007).
71. O. Lehnert, J. Frýda, W. Buggisch, A. Munnecke, A. Nützel, J. Kříž, S. Manda, $\delta^{13}C$ records across the late Silurian Lau event: New data from middle palaeo-latitudes of northern peri-Gondwana (Prague Basin, Czech Republic). *Palaeogeogr. Palaeoclimatol. Palaeoecol.* **245**, 227–244 (2007).
72. B. D. Cramer, M. D. Schmitz, W. D. Huff, S. M. Bergström, High-precision U-Pb zircon age constraints on the duration of rapid biogeochemical events during the Ludlow Epoch (Silurian Period). *J. Geol. Soc. London* **172**, 157–160 (2015).
73. M. M. Joachimski, R. D. Pancost, K. H. Freeman, C. Ostertag-Henning, W. Buggisch, Carbon isotope geochemistry of the Frasnian–Famennian transition. *Palaeogeogr. Palaeoclimatol. Palaeoecol.* **181**, 91–109 (2002).
74. W. Buggisch, M. M. Joachimski, Carbon isotope stratigraphy of the Devonian of Central and Southern Europe. *Palaeogeogr. Palaeoclimatol. Palaeoecol.* **240**, 68–88 (2006).
75. W. Buggisch, M. M. Joachimski, G. Sevastopulo, J. R. Morrow, Mississippian $\delta^{13}C$ carb and conodont apatite $\delta^{18}O$ records—Their relation to the Late Palaeozoic Glaciation. *Palaeogeogr. Palaeoclimatol. Palaeoecol.* **268**, 273–292 (2008).
76. D. P. G. Bond, P. B. Wignall, W. Wang, G. Izon, H.-S. Jiang, X.-L. Lai, Y.-D. Sun, R. J. Newton, L.-Y. Shao, S. Védrine, H. Cope, The mid-Capitanian (Middle Permian) mass extinction and carbon isotope record of South China. *Palaeogeogr. Palaeoclimatol. Palaeoecol.* **292**, 282–294 (2010).
77. D. P. G. Bond, J. Hilton, P. B. Wignall, J. R. Ali, L. G. Stevens, Y. Sun, X. Lai, The Middle Permian (Capitanian) mass extinction on land and in the oceans. *Earth Sci. Rev.* **102**, 100–116 (2010).
78. P. B. Wignall, Y. Sun, D. P. G. Bond, G. Izon, R. J. Newton, S. Védrine, M. Widdowson, J. R. Ali, X. Lai, H. Jiang, H. Cope, S. H. Bottrell, Volcanism, mass extinction, and carbon isotope fluctuations in the Middle Permian of China. *Science* **324**, 1179–1182 (2009).
79. C. Cao, G. D. Love, L. E. Hays, W. Wang, S. Shen, R. E. Summons, Biogeochemical evidence for euxinic oceans and ecological disturbance presaging the end-Permian mass extinction event. *Earth Planet. Sci. Lett.* **281**, 188–201 (2009).
80. J. L. Payne, D. J. Lehrmann, J. Wei, M. J. Orchard, D. P. Schrag, A. H. Knoll, Large perturbations of the carbon cycle during recovery from the end-Permian extinction. *Science* **305**, 506–509 (2004).
81. F. A. Corsetti, A. Baud, P. J. Marenco, S. Richoz, Summary of Early Triassic carbon isotope records. *C. R. Palevol* **4**, 473–486 (2005).
82. T. Galfetti, H. Bucher, A. Brayard, P. A. Hochuli, H. Weissert, K. Guodun, V. Atudorei, J. Guex, Late Early Triassic climate change: Insights from carbonate carbon isotopes, sedimentary evolution and ammonoid paleobiogeography. *Palaeogeogr. Palaeoclimatol. Palaeoecol.* **243**, 394–411 (2007).
83. T. Galfetti, H. Bucher, M. Ovtcharova, U. Schaltegger, A. Brayard, T. Brühwiler, N. Goudemand, H. Weissert, P. A. Hochuli, F. Cordey, K. Guodun, Timing of the Early Triassic carbon cycle perturbations inferred from new U–Pb ages and ammonoid biochronozones. *Earth Planet. Sci. Lett.* **258**, 593–604 (2007).
84. S. P. Hesselbo, S. A. Robinson, F. Surlyk, S. Piasecki, Terrestrial and marine extinction at the Triassic-Jurassic boundary synchronized with major carbon-cycle perturbation: A link to initiation of massive volcanism? *Geology* **30**, 251–254 (2002).
85. M. Ruhl, M. H. L. Deenen, H. A. Abels, N. R. Bonis, W. Krijgsman, W. M. Kürschner, Astronomical constraints on the duration of the early Jurassic Hettangian stage and recovery rates following the end-Triassic mass extinction (St Audrie's Bay/East Quantoxhead, UK). *Earth Planet. Sci. Lett.* **295**, 262–276 (2010).
86. C. Korte, H. W. Kozur, Bio- and chemostratigraphic assessment of carbon isotope records across the Triassic–Jurassic boundary at Csővár quarry (Hungary) and Kendlbachgraben (Austria) and implications for global correlations. *Bull. Geol. Soc. Denmark* **59**, 101–115 (2011).
87. A. Bachan, B. van de Schootbrugge, J. L. Payne, The end-Triassic negative $\delta^{13}C$ excursion: A lithologic test. *Palaeogeogr. Palaeoclimatol. Palaeoecol.* **412**, 177–186 (2014).
88. C. A. McRoberts, H. Furrer, D. S. Jones, Palaeoenvironmental interpretation of a Triassic-Jurassic boundary section from Western Austria based on palaeoecological and geochemical data. *Palaeogeogr. Palaeoclimatol. Palaeoecol.* **136**, 79–95 (1997).
89. M. T. Galli, F. Jadoul, S. M. Bernasconi, H. Weissert, Anomalies in global carbon cycling and extinction at the Triassic/Jurassic boundary: Evidence from a marine C-isotope record. *Palaeogeogr. Palaeoclimatol. Palaeoecol.* **216**, 203–214 (2005).
90. J. Pálfy, A. Demény, J. Haas, E. S. Carter, A. Görög, D. Halász, A. Oravecz-Scheffer, M. Hetényi, E. Márton, M. J. Orchard, P. Ozsvárt, I. Vető, N. Zajzon, Triassic–Jurassic boundary events inferred from integrated stratigraphy of the Csővár section, Hungary. *Palaeogeogr. Palaeoclimatol. Palaeoecol.* **244**, 11–33 (2007).
91. C. Korte, S. P. Hesselbo, H. C. Jenkyns, R. E. M. Rickaby, C. Spötl, Palaeoenvironmental significance of carbon- and oxygen-isotope stratigraphy of marine Triassic–Jurassic boundary sections in SW Britain. *J. Geol. Soc. London* **166**, 431–445 (2009).
92. M.-E. Clémence, S. Gardin, A. Bartolini, G. Paris, V. Beaumont, J. Guex, Bentho-planktonic evidence from the Austrian Alps for a decline in sea-surface carbonate production at the end of the Triassic. *Swiss J. Geosci.* **103**, 293–315 (2010).
93. M.-E. Clémence, A. Bartolini, S. Gardin, G. Paris, V. Beaumont, K. N. Page, Early Hettangian benthic–planktonic coupling at Doniford (SW England): Palaeoenvironmental implications for the aftermath of the end-Triassic crisis. *Palaeogeogr. Palaeoclimatol. Palaeoecol.* **295**, 102–115 (2010).
94. S. E. Greene, R. C. Martindale, K. A. Ritterbush, D. J. Bottjer, F. A. Corsetti, W. M. Berelson, Recognising ocean acidification in deep time: An evaluation of the evidence for acidification across the Triassic-Jurassic boundary. *Earth Sci. Rev.* **113**, 72–93 (2012).
95. H. C. Jenkyns, The early Toarcian (Jurassic) anoxic event: Stratigraphic, sedimentary, and geochemical evidence. *Am. J. Sci.* **288**, 101–151 (1988).
96. S. P. Hesselbo, H. C. Jenkyns, L. V. Duarte, L. C. V. Oliveira, Carbon-isotope record of the Early Jurassic (Toarcian) Oceanic Anoxic Event from fossil wood and marine carbonate (Lusitanian Basin, Portugal). *Earth Planet. Sci. Lett.* **253**, 455–470 (2007).
97. G. Suan, B. Pittet, I. Bour, E. Mattioli, L. V. Duarte, S. Mailliot, Duration of the Early Toarcian carbon isotope excursion deduced from spectral analysis: Consequence for its possible causes. *Earth Planet. Sci. Lett.* **267**, 666–679 (2008).
98. M. Hermoso, L. Le Callonnec, F. Minoletti, M. Renard, S. P. Hesselbo, Expression of the Early Toarcian negative carbon-isotope excursion in separated carbonate microfractions (Jurassic, Paris Basin). *Earth Planet. Sci. Lett.* **277**, 194–203 (2009).
99. B. Pittet, G. Suan, F. Lenoir, L. V. Duarte, E. Mattioli, Carbon isotope evidence for sedimentary discontinuities in the lower Toarcian of the Lusitanian Basin (Portugal): Sea level change at the onset of the Oceanic Anoxic Event. *Sediment. Geol.* **303**, 1–14 (2014).
100. C. Huang, S. P. Hesselbo, Pacing of the Toarcian Oceanic Anoxic Event (Early Jurassic) from astronomical correlation of marine sections. *Gondw. Res.* **25**, 1348–1356 (2014).
101. S. D. Burgess, S. A. Bowring, T. H. Fleming, D. H. Elliot, High-precision geochronology links the Ferrar large igneous province with early-Jurassic ocean anoxia and biotic crisis. *Earth Planet. Sci. Lett.* **415**, 90–99 (2015).
102. A. P. Menegatti, H. Weissert, R. S. Brown, R. V. Tyson, P. Farrimond, A. Strasser, M. Caron, High-resolution $\delta^{13}C$ stratigraphy through the Early Aptian "Livello selli" of the Alpine Tethys. *Paleoceanography* **13**, 530–545 (1998).
103. E. Erba, J. E. T. Channell, M. Claps, C. Jones, R. Larson, B. Opdyke, I. P. Silva, A. Riva, G. Salvini, S. Torricelli, Integrated stratigraphy of the Cismon Apticore (southern Alps, Italy); a "reference section" for the Barremian-Aptian interval at low latitudes. *J. Foramin. Res.* **29**, 371–391 (1999).
104. A. Bellanca, E. Erba, R. Neri, I. P. Silva, M. Sprovieri, F. Tremolada, D. Verga, Palaeoceanographic significance of the Tethyan 'Livello Selli' (Early Aptian) from the Hybla Formation, northwestern Sicily: Biostratigraphy and high-resolution chemostratigraphic records. *Palaeogeogr. Palaeoclimatol. Palaeoecol.* **185**, 175–196 (2002).
105. G. D. Price, New constraints upon isotope variation during the early Cretaceous (Barremian–Cenomanian) from the Pacific Ocean. *Geol. Mag.* **140**, 513–522 (2003).

106. A. Malinverno, E. Erba, T. D. Herbert, Orbital tuning as an inverse problem: Chronology of the early Aptian oceanic anoxic event 1a (Selli Level) in the Cismon APTICORE. *Paleoceanography* **25**, PA2203 (2010).
107. I. Jarvis, A. S. Gale, H. C. Jenkyns, M. A. Pearce, Secular variation in Late Cretaceous carbon isotopes: A new $\delta^{13}C$ carbonate reference curve for the Cenomanian–Campanian (99.6–70.6 Ma). *Geol. Mag.* **143**, 561–608 (2006).
108. A. Ando, B. T. Huber, K. G. MacLeod, Depth-habitat reorganization of planktonic foraminifera across the Albian/Cenomanian boundary. *Paleobiology* **36**, 357–373 (2010).
109. B. T. Huber, R. D. Norris, K. G. MacLeod, Deep-sea paleotemperature record of extreme warmth during the Cretaceous. *Geology* **30**, 123–126 (2002).
110. A. Ando, B. T. Huber, K. G. MacLeod, T. Ohta, B.-K. Khim, Blake Nose stable isotopic evidence against the mid-Cenomanian glaciation hypothesis. *Geology* **37**, 451–454 (2009).
111. Y. J. Joo, B. B. Sageman, Cenomanian to Campanian carbon isotope chemostratigraphy from the Western Interior Basin, U.S.A. *J. Sediment. Res.* **84**, 529–542 (2014).
112. J. S. Eldrett, C. Ma, S. C. Bergman, B. Lutz, F. J. Gregory, P. Dodsworth, M. Phipps, P. Hardas, D. Minisini, A. Ozkan, J. Ramezani, S. A. Bowring, S. L. Kamo, K. Ferguson, C. Macaulay, A. E. Kelly, An astronomically calibrated stratigraphy of the Cenomanian, Turonian and earliest Coniacian from the Cretaceous Western Interior Seaway, USA: Implications for global chronostratigraphy. *Cretaceous Res.* **56**, 316–344 (2015).
113. L. Alegret, E. Thomas, K. C. Lohmann, End-Cretaceous marine mass extinction not caused by productivity collapse. *Proc. Natl. Acad. Sci. U.S.A.* **109**, 728–732 (2012).
114. T. Westerhold, U. Röhl, I. Raffi, E. Fornaciari, S. Monechi, V. Reale, J. Bowles, H. F. Evans, Astronomical calibration of the Paleocene time. *Palaeogeogr. Palaeoclimatol. Palaeoecol.* **257**, 377–403 (2008).
115. K. Littler, U. Röhl, T. Westerhold, J. C. Zachos, A high-resolution benthic stable-isotope record for the South Atlantic: Implications for orbital-scale changes in Late Paleocene–Early Eocene climate and carbon cycling. *Earth Planet. Sci. Lett.* **401**, 18–30 (2014).
116. G. Bernaola, J. I. Baceta, X. Orue-Etxebarria, L. Alegret, M. Martín-Rubio, J. Arostegui, J. Dinarès-Turell, Evidence of an abrupt environmental disruption during the mid-Paleocene biotic event (Zumaia section, western Pyrenees). *Geol. Soc. Am. Bull.* **119**, 785–795 (2007).
117. U. Röhl, T. Westerhold, T. J. Bralower, J. C. Zachos, On the duration of the Paleocene-Eocene thermal maximum (PETM). *Geochem. Geophys. Geosyst.* **8**, Q12002 (2007).
118. K. A. Farley, S. F. Eltgroth, An alternative age model for the Paleocene–Eocene thermal maximum using extraterrestrial ^{3}He. *Earth Planet. Sci. Lett.* **208**, 135–148 (2003).
119. B. H. Murphy, K. A. Farley, J. C. Zachos, An extraterrestrial ^{3}He-based timescale for the Paleocene–Eocene thermal maximum (PETM) from Walvis Ridge, IODP Site 1266. *Geochim. Cosmochim. Acta* **74**, 5098–5108 (2010).
120. H. McCarren, E. Thomas, T. Hasegawa, U. Röhl, J. C. Zachos, Depth dependency of the Paleocene-Eocene carbon isotope excursion: Paired benthic and terrestrial biomarker records (Ocean Drilling Program Leg 208, Walvis Ridge). *Geochem. Geophys. Geosyst.* **9**, Q10008 (2008).
121. S. K. Turner, A. Ridgwell, Development of a novel empirical framework for interpreting geological carbon isotope excursions, with implications for the rate of carbon injection across the PETM. *Earth Planet. Sci. Lett.* **435**, 1–13 (2016).
122. L. Stap, A. Sluijs, E. Thomas, L. Lourens, Patterns and magnitude of deep sea carbonate dissolution during Eocene Thermal Maximum 2 and H2, Walvis Ridge, southeastern Atlantic Ocean. *Paleoceanography* **24**, PA1211 (2009).
123. V. Lauretano, K. Littler, M. Polling, J. C. Zachos, L. J. Lourens, Frequency, magnitude and character of hyperthermal events at the onset of the Early Eocene Climatic Optimum. *Climate Past Discuss.* **11**, 1313–1324 (2015).
124. J. C. Zachos, T. M. Quinn, K. A. Salamy, High-resolution (10^4 years) deep-sea foraminiferal stable isotope records of the Eocene-Oligocene climate transition. *Paleoceanography* **11**, 251–266 (1996).
125. H. K. Coxall, P. A. Wilson, H. Pälike, C. H. Lear, J. Backman, Rapid stepwise onset of Antarctic glaciation and deeper calcite compensation in the Pacific Ocean. *Nature* **433**, 53–57 (2005).
126. J. C. Zachos, L. R. Kump, Carbon cycle feedbacks and the initiation of Antarctic glaciation in the earliest Oligocene. *Global Planet. Change* **47**, 51–66 (2005).
127. A. Holbourn, W. Kuhnt, K. G. D. Kochhann, N. Andersen, K. J. S. Meier, Global perturbation of the carbon cycle at the onset of the Miocene Climatic Optimum. *Geology* **43**, 123–126 (2015).
128. A. Holbourn, W. Kuhnt, S. Clemens, W. Prell, N. Andersen, Middle to late Miocene stepwise climate cooling: Evidence from a high-resolution deep water isotope curve spanning 8 million years. *Paleoceanography* **28**, 688–699 (2013).
129. A. Holbourn, W. Kuhnt, M. Lyle, L. Schneider, O. Romero, N. Andersen, Middle Miocene climate cooling linked to intensification of eastern equatorial Pacific upwelling. *Geology* **42**, 19–22 (2014).
130. C. D. Peterson, L. E. Lisiecki, J. V. Stern, Deglacial whole-ocean $\delta^{13}C$ change estimated from 480 benthic foraminiferal records. *Paleoceanography* **29**, 549–563 (2014).
131. D. H. Rothman, J. M. Hayes, R. E. Summons, Dynamics of the Neoproterozoic carbon cycle. *Proc. Natl. Acad. Sci. U.S.A.* **100**, 8124–8129 (2003).
132. D. H. Rothman, G. P. Fournier, K. L. French, E. J. Alm, E. A. Boyle, C. Cao, R. E. Summons, Methanogenic burst in the end-Permian carbon cycle. *Proc. Natl. Acad. Sci. U.S.A.* **111**, 5462–5467 (2014).
133. S. R. Emerson, J. I. Hedges, *Chemical Oceanography and the Marine Carbon Cycle* (Cambridge Univ. Press, 2008).
134. R. A. Berner, *The Phanerozoic Carbon Cycle: CO_2 and O_2* (Oxford Univ. Press, 2004).
135. F. T. Mackenzie, A. Lerman, *Carbon in the Geobiosphere: Earth's Outer Shell* (Springer, 2006).

Acknowledgments: This project was inspired by a great many discussions with S. Bowring. I thank him for generously sharing his insight into geologic time, the intellectual history of mass extinction, and the present understanding of the "sixth extinction." I also thank T. Bosak, O. Devauchelle, R. Ferrari, L. Hatton, J. Hayes, P. Molnar, and R. Summons for helpful discussions. **Funding:** This work was supported by NASA Astrobiology grant NNA13AA90A and NSF grant EAR-1338810. **Competing interests:** The author declares that he has no competing interests. **Data and materials availability:** All data needed to evaluate the conclusions in the paper are present in the paper. Additional data related to this paper may be requested from the author.

Submitted 20 March 2017
Accepted 24 August 2017
Published 20 September 2017
10.1126/sciadv.1700906

Citation: D. H. Rothman, Thresholds of catastrophe in the Earth system. *Sci. Adv.* **3**, e1700906 (2017).

ScienceAdvances

Thresholds of catastrophe in the Earth system

Daniel H. Rothman

Sci Adv **3** (9), e1700906.
DOI: 10.1126/sciadv.1700906